



Electronic processes in molecular dynamics simulations of nanoscale metal tips under electric fields

S. Parviainen ^{a,*}, F. Djurabekova ^a, H. Timko ^{a,b}, K. Nordlund ^a

^a Department of Physics and Helsinki Institute of Physics, P.O. Box 43, University of Helsinki, FIN-00014 Helsinki, Finland

^b CERN, Genève 23, CH-1211, Switzerland

ARTICLE INFO

Article history:

Received 31 May 2010

Received in revised form 28 January 2011

Accepted 9 February 2011

Available online 21 March 2011

Keywords:

Molecular dynamics

Electronic effects

Resistive heating

Thermal conduction

ABSTRACT

Electronic effects play a crucial role in the temperature evolution of metal parts which have electric currents running through them. The increase in temperature due to resistive heating can cause the melting of metal nanoscale wires creating damage in electric circuits. Likewise, electric currents are also present in sharp features on metal surfaces exposed to high electric fields. The destruction of such tips can lead to vacuum arcs, supplying the neutral species to build up plasma over the surface. To follow the temperature evolution caused by electric currents in such a tip, we developed a new model, based on an existing molecular dynamics code, to include resistive heating and electronic thermal conduction. The results given by the new simulation model are in good agreement with analytical predictions.

© 2011 Published by Elsevier B.V.

1. Introduction

Electric currents running through tips on a metal surface can modify the shape of the tips significantly, even leading to their melting, if the surface is exposed to a sufficiently high electric field. These strong electric fields appear in connection with many modern applications operated at high vacuums, such as particle accelerators and fusion reactors, causing the undesirable effect of electric arcs. In many cases these arcs can damage sensitive parts, such as particle accelerator structures [1,2], or field ion microscopy specimens [3], leading to lowered device performance. On the other hand, the same phenomenon is deliberately utilized in, e.g. metal vapor vacuum arc (MEVVA) ion sources [4] which are used in ion implantation, thin film deposition and particle accelerators.

Even though vacuum arcs have already been under scientific inquiry for decades [5,6], the onset of arcing is not well understood, and simulations of the processes possibly leading to arcing may help to gain a better understanding of this complex phenomenon.

It has been suggested that electron emission, especially field electron emission [7], from protrusions on a surface plays a significant role in the stages leading up to arcing.

It is believed that electron emission from sharp, tip shaped emitters on the surface result in local melting of the surface, causing atoms to be evaporated. At the same time, due to geometric effects, the tip can enhance the electric field above it

to values at which the tip starts to break due to field evaporation [8,9]. This process results in plasma build-up and electric arcing [10].

In order to be able to simulate the electronic effects using a molecular dynamics (MD) code, a model for the dynamic evolution of the lattice temperature in the emitter tip, as a result of resistive heating and thermal conduction, is required. Previous models that include electronic thermal conduction effects based on electron phonon coupling (EPC) [11–14] were developed for the simulation of interactions of highly energetic ions with an electronic environment. These models consider a bulk material in an extreme nonequilibrium state, for example during the development of thermal spikes. Therefore, these models are not suitable in simulations of slow, near equilibrium heating processes, such as the resistive heating which is responsible for the temperature evolution in tips exposed to high electric fields.

The present model assumes an initially symmetric copper tip of cylindrical shape on a copper surface. Because of the cylindrical symmetry, a 1D geometry can be used to model the heat flow in the tip. During the simulation, the tip is allowed to change its shape slightly due to effects such as relaxation and thermal expansion, according to MD simulations.

In the next section we will give a brief overview of the theoretical model we use, the various effects that we consider, and some details of how these were implemented in the PARCAS [15,16] MD code. The results obtained for a copper {100} surface with a tip of a cylindrical shape are discussed and compared to analytical predictions in the results section. To simulate the copper structure, the Sabochick and Lam [17] EAM potential was used with a

* Corresponding author. Tel.: +358 9 19150003.

E-mail address: stefan.parviainen@helsinki.fi (S. Parviainen).

constant timestep $\Delta t = 4.05$ fs and periodic boundaries in the bulk surface plane. The size of the bulk surface varied from $11.5 \text{ nm} \times 11.5 \text{ nm}$ to $28.9 \text{ nm} \times 28.9 \text{ nm}$ depending on the size of simulated tip.

2. Theoretical model

2.1. Electron emission

In a free-electron model, electrons are free to move inside a metal, but to escape from the metal, they must overcome the work function potential energy barrier ϕ . This can be achieved by raising the energy of the electrons (*thermal emission* and *photoemission*) or by applying a high electric field above the surface which lowers the energy barrier and makes it narrower, increasing the probability of electrons to tunnel through it and to escape from the surface (*field emission*).

Due to field enhancement around the emission site, the local electric field directly above the tip is given by

$$F = \beta_{FN} E, \quad (1)$$

where β_{FN} is the field enhancement factor and E is the applied macroscopic field. At high local fields the field emission is dominant [18] compared to the other emission forms, and thus the total electron current can be approximated by the Fowler–Nordheim (FN) equation

$$J(F, T) = \lambda_T \frac{aF^2}{\phi\tau(F)^2} \exp\left(-v(F) \frac{b\phi^{3/2}}{F}\right) \quad (2)$$

where λ_T is a temperature correction factor given below and $a = 1.54 \frac{\text{ÅV}}{\text{eV}^2}$ and $b = 6.83 \frac{\text{V}}{\text{eV}^{3/2}\text{nm}}$ are the first and second Fowler–Nordheim constants respectively, and τ and v are correction factors that depend on the shape of the energy barrier the electrons have to tunnel through to escape from the surface. In our model we assume a Schottky–Nordheim barrier [19].

As the temperature rises, the contribution of thermally emitted electrons becomes significant. This is taken into account by including the temperature correction factor

$$\lambda_T = \frac{\pi k_B T / d_T}{\sin(\pi k_B T / d_T)}, \quad (3)$$

where $d_T = \frac{2F}{3b\sqrt{\phi}}$ is the decay width of the energy barrier and k_B is Boltzmann's constant [20,18].

Since the Fowler–Nordheim equation plays an important part in our model, its limitations must be considered carefully. Eq. (2) only gives reliable predictions within a certain range of fields and lattice temperatures [18], and, thus, if the problem deals with these parameters beyond the range of validity, it is recommended to use, e.g. the General Thermal Field (GTF) equation [21] instead. In our model, this is, however, not the case and thus the more advanced models are outside of the scope of this paper.

2.2. Space charge screening

High electric currents leaving the surface tips form a space charge, which affects the value of the electric field between the electrodes, reducing the current density of the emitted current. Since the actual value of the current flowing through the tip is of great importance in our model, some attention must be given to the space charge screening phenomenon.

The effect of space charge on the electric field can be estimated accurately by solving Poisson's equation [22] for a given tip geometry. In this case it is, however, necessary to calculate the charge distribution due to the emitted electrons, which is not possible

to accomplish in conventional MD simulations. The screening effect can also be estimated by considering a simplified planar geometry, in which case an analytical expression is found for the field reduction [23] (for instance, a reduction by 20% was found for the local electric field $F = 8 \frac{\text{ÅV}}{\text{m}}$ and the voltage $V = 5$ kV between the electrodes).

In the present model the effect of space charge on the current density is ignored, because of the difficulty in accurately estimating the screening effect for dynamically changing tips in MD. However, we note that it would be possible to account for the effect by calculating the reduction of the current density using Particle-In-Cell (PIC) simulations [10], either by linking MD and PIC concurrently, or by scaling the electric field in the MD based on results from separate PIC simulations done for similar tips and current.

2.3. Resistive heating

Electron emission gives rise to an electric current, which, due to resistive heating, increases the temperature of the tip. Because of the dynamic heating, the tip temperature varies considerably during simulations and, therefore, our model must work over a wide range of temperatures. To meet this requirement, we account for the temperature dependence of resistivity by using the model developed by Matula et al. [24] and later improved by Schuster et al. [25]. In this model the resistivity is given by

$$\rho(T) = A \left[1 + \frac{BT}{\theta'} + D \left(\frac{\theta'}{T} \right)^p \right] \Phi \left(\frac{\theta'}{T} \right) + \rho_0, \quad (4)$$

where $A = 1.816013 \mu\Omega \text{ cm}$, $B = -2.404851 \times 10^{-3}$, $C = 4.560643 \times 10^{-2}$, $D = -5.976831 \times 10^{-3}$, $p = -1.838419$, and $\rho_R = 1.803752 \times 10^{-4} \mu\Omega \text{ cm}$ are constants as given in [25], $\theta' = 310.8 \text{ K} - CT$, and

$$\Phi(x) = \frac{4}{x^5} \int_0^x \frac{z^5 e^z}{(e^z - 1)^2} dz. \quad (5)$$

For nanoscale protrusions, where the diameter is less than the mean free path of electrons, finite size effects become considerable. Using a previously developed code [26] we calculated the resistivity of copper nanowires of various thicknesses at the temperature $T = 300$ K. In the code, the probability of specular reflection of electrons from the tip walls was taken to be 1%, which is close to values reported in literature [27,28]. We assume that the finite size effect does not depend on temperature, and thus the corrected resistivity is given by

$$\rho(T)_{\text{corr}} = \frac{\rho(300 \text{ K})_{\text{corr}}}{\rho(300 \text{ K})_{\text{bulk}}} \rho(T)_{\text{bulk}}. \quad (6)$$

Due to finite size effects, the resistivity was found to be up to 13 times higher than the bulk value for a tip with a diameter of 5 nm and up to 65 times higher for a wire with a diameter of 1 nm.

2.4. Thermal radiation

Some of the heat energy generated due to resistive heating is lost in the form of thermal radiation. Since we assume tips of cylindrical shape, we can approximate this kind of energy loss as

$$P_{BB} = -\sigma_B A T^4 = -\pi \sigma_B r (2h + r) T^4, \quad (7)$$

where $\sigma_B = 5.67 \times 10^{-8} \text{ W m}^{-2} \text{ K}^{-4}$ is the Stefan–Boltzmann constant and T is assumed to be constant throughout the tip. The assumption of a constant temperature gives an upper limit for the radiation; in reality a temperature gradient caused by thermal conduction exists, and the temperature at the base of the tip is much lower than the temperature at the top.

The energy loss due to thermal radiation is often orders of magnitude smaller than the energy added due to resistive

heating. Assuming a tip with height 100 nm and diameter 5 nm at temperature $T = 1000$ K, the power lost due to radiation is less than 90 pW, while 390 nW is generated due to resistive heating in the presence of a local field $F = 8 \frac{\text{eV}}{\text{m}}$. Moreover, in finite-sized objects the emissivity is typically much below one [29], which reduces the thermal radiation even further. At high electric fields we can, thus, safely assume that thermal radiation is negligible and it is, therefore, ignored in our model.

2.5. Thermal conduction

The main process competing with resistive heating, and preventing an immediate temperature rise in tips, is thermal conduction, which strives to lower the temperature of the tip. In the model we use, the bulk surface, which the tip is attached to, acts as a heat bath that keeps the bottom of the tip at a constant temperature, while the top of the tip is thermally isolated.

Thermal conduction can be divided into two main components: lattice thermal conduction, caused by interatomic interactions, and electronic thermal conduction, due to electronic effects. Classical MD implicitly handles only lattice conduction [30], even though electronic conduction usually dominates in metals [31].

To handle the electronic conductivity consistently within a classical MD code, our model explicitly includes the electronic component by considering the macroscopic diffusion equation

$$\frac{\partial T(x, t)}{\partial t} = \frac{\kappa_e}{C_V} \frac{\partial^2 T(x, t)}{\partial x^2}, \quad (8)$$

where κ_e is the electronic thermal conductivity and C_V the volumetric heat capacity of the tip material. When resistive heating is also included, the full heat equation of the tip can be written as

$$\frac{\partial T}{\partial t} = \frac{1}{C_V} \left(\rho(T) J(x)^2 + \kappa_e \frac{\partial^2 T}{\partial x^2} \right). \quad (9)$$

The tip temperature can thus be obtained during simulations by solving Eq. (9) numerically. The equation is solved in 1D based on cylindrical symmetry.

The thermal conductivity is also affected by finite size effects [32]. In our model, the electronic component of the thermal conductivity is calculated based on the Wiedemann–Franz law

$$\kappa_e = \frac{LT}{\rho(T)}, \quad (10)$$

where $L = 23 \frac{\text{nW}\Omega}{\text{K}^2}$ is the Lorenz number [33]. The finite size effect is included by using the resistivity value obtained from Eq. (6) in Eq. (10). As indicated by Eq. (10) the thermal conductivity depends on the temperature. However, we approximated the thermal conductivity by a constant value obtained at the room temperature. The simplification was motivated by the fact that the strong temperature dependence of the resistivity is partially compensated by the value of the temperature (Eq. 10). The calculation of the actual dependence over the temperature range $T = 300\text{--}1200$ K showed that the thermal conductivity varies by only about 20%. Taking into account the fluctuations due to the dynamic calculations, for simplicity it can be, thus, taken as a constant.

2.6. Analytical solution

The analytical solution of Eq. (9) allows for the analysis of the temperature evolution in a tip, even when the aspect ratio of the tip grows larger than what can be simulated using an MD code. The analytical solution can also be used for the verification of simulation results.

If instead of Eq. (4), a linear approximation is used to calculate the resistivity, Eq. (9) has an analytical solution which gives the equilibrium temperature of the apex of the tip as

$$T_m = T_B \sec \left(\sqrt{\frac{\rho_R}{\kappa T_R}} Jh \right), \quad (11)$$

where T_B is the temperature at the base of the tip and h is the height of the tip, both assumed to be constants, and ρ_R is the resistivity at some reference temperature T_R [34]. If, furthermore, the resistivity is assumed to be inversely proportional to the tip radius, i.e.

$$\rho = \frac{a\rho_R T}{T_R r}, \quad (12)$$

where r is the radius and a is some constant determined, e.g. by fitting a line to inverse resistivity values determined by some more accurate method such as computer simulations [35], Eq. (11) takes the form

$$T_m = T_B \sec \left(\frac{\rho_R}{T_R \sqrt{L}} J\beta \right), \quad (13)$$

where $\beta = \frac{h}{r}$ is the aspect ratio of the tip. In the range $0.5 \text{ nm} < r < 10 \text{ nm}$ this approximation is correct to $\pm 6\%$ when $a = 70 \text{ nm}$.

It should be noted that β in Eq. (13) is not necessarily equal to the field enhancement factor β_{FN} , although this is a common approximation. The exact dependence of the field enhancement factor β_{FN} on the tip aspect ratio β remains unclear. Commonly cited values include $\beta_{FN} = 3 + \beta$ [36] and $\beta_{FN} = 0.73\beta + 5.93$ [9]. However, for the purpose of estimating the temperature evolution in an emitter tip, assuming $\beta_{FN} = \beta$ is a simple and good approximation which is also used in the present work.

2.7. Implementation details

Because the geometry of a simulated tip may change during simulation, it is not possible to assume that the emission current density remains constant during simulations. To handle the dynamic geometry, the heated tip is divided into separate, discrete columns, each with the same cross-section area, but of varying height. The electric field above each column is calculated by numerically solving Laplace's equation [37]. Eq. (2) is then used to calculate the density of the current passing through the column, towards the top.

The tip temperature is adjusted every simulation time step so that it matches the distribution given by Eq. (9), which is solved numerically using the finite difference method [38]. Adjusting the temperature is accomplished by directly scaling the atomic velocities for all the atoms on a given height in the tip by a scaling factor

$$\alpha = \sqrt{\frac{T_2}{T_1}}, \quad (14)$$

where T_2 is the new temperature and T_1 the old temperature of the atom. Because the velocities are simply scaled, the direction of the atomic movement is preserved.

3. Results

To verify the model used and its implementation, simulation results using this model were compared with predictions based on the analytical solution of the heat equation. In the analytical calculations an estimated lattice conductivity $3 \frac{\text{W}}{\text{mK}}$ were added to the electronic thermal conductivity given by Eq. (10) to obtain the total thermal conduction. Our estimate for the lattice conductivity is of the same order as previous estimates [39].

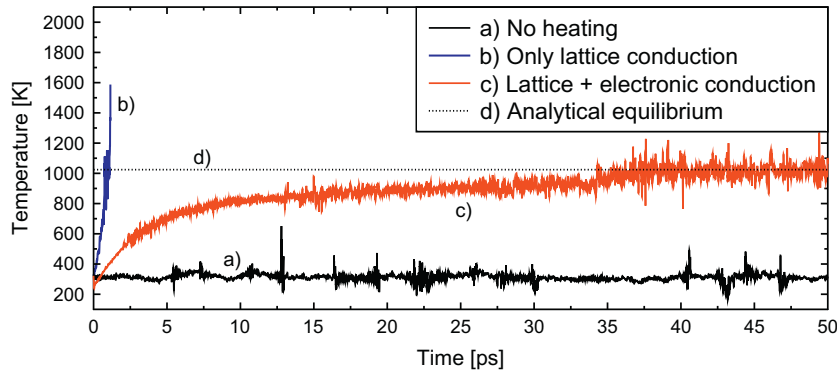


Fig. 1. Evolution of apex temperature of a tip with final height 13.1 nm and diameter 2 nm when a constant current of density $7.9 \times 10^{-6} \frac{\text{A}}{\text{nm}^2}$ passes through it. The temperature approaches the analytically predicted value 1033 K only when both lattice and electronic conduction are included.

Fig. 1 shows the evolution of the apex temperature of a tip during simulation runs using different heat conduction schemes. It is clearly seen that the temperature increase is vastly overestimated if the electronic contribution to thermal conductivity is ignored, while the temperature curve reaches the level of the analytical prediction after ≈ 40 ps if both lattice and electronic conduction are considered. A constant current density was used to make comparison with the analytical solution easier.

The model was also tested by heating tips of various heights with the assumption of a constant current density for comparisons with the analytical predictions. Fig. 2 shows both equilibrium temperatures as obtained by simulations and by Eq. (11). Although the temperature fluctuations at high temperatures were fairly high in the simulations, the obtained temperatures are very close to the analytical predictions.

Thermal instability, known as Rayleigh instability [40], may break nanowires at temperatures as low as 670 K [41], while the bulk melting temperature is 1295 K according to the Sabochick–Lam potential used. We also observed a similar phenomenon leading to the formation of a clearly thinner part of the tip in some simulations (Fig. 3), which suggests that there is a probability that even a moderate temperature increase may lead to the formation of large atom clusters detached from the tip. However, the impact of the instability on field evaporation rates was not investigated further.

When finite size effects are accounted for, the maximum temperature a tip can reach depends only on the emission current density and the tip aspect ratio. If, furthermore, it is assumed that the enhancement of the applied field above the tip is purely

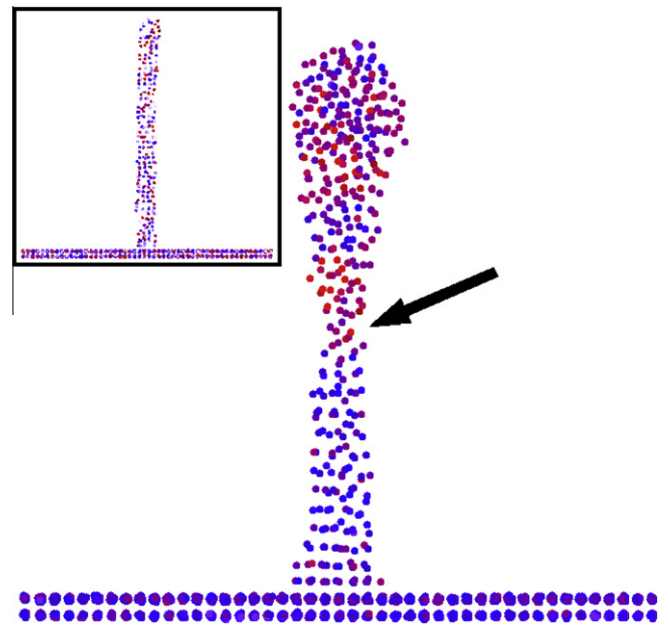


Fig. 3. Tip shape after resistive heating (inset shows original tip shape after relaxation). The middle part of the tip has become narrower due to Rayleigh instability.

geometrical, and that the enhancement factor is given by the aspect ratio of the tip, it is seen that the reached temperature depends only on the aspect ratio and the applied field.

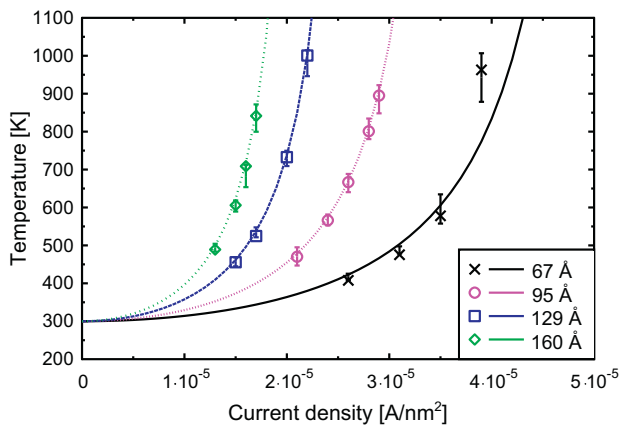


Fig. 2. Tip temperature as a function of current density. The symbols indicate analytical predictions while the bars indicate simulation results. Lines indicate expected behavior assuming the tip height does not change during simulation.

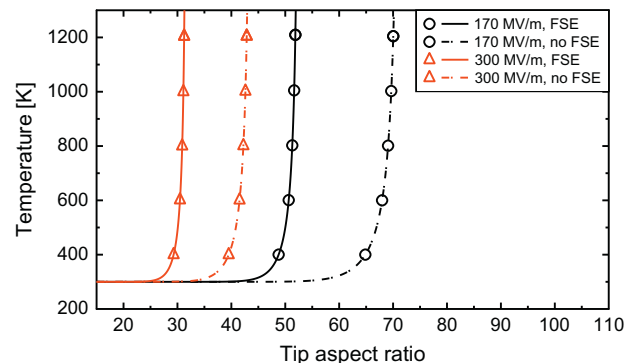


Fig. 4. Maximum tip temperature as a function of tip aspect ratio when an external electric field is applied. Finite size effects (FSE) are considered for the solid lines, while the effects have been ignored for the dotted lines. The field enhancement factor is assumed to be given by the tip aspect ratio.

According to experiments, breakdowns on conditioned copper surfaces occur when an external field of $E \approx 170 \frac{\text{MV}}{\text{m}}$ is applied. During the experiments a field enhancement factor of $\beta \approx 50$ is measured [2]. As shown in Fig. 4, such values lead to the melting of the tip when it is assumed that the field enhancement factor is given directly by the tip aspect ratio and finite size effects are considered, suggesting that tip melting is indeed an important factor in breakdowns, as suggested previously. However, for unconditioned surfaces enhancement factors of $\beta \approx 20$ and breakdown fields of $E \approx 300 \frac{\text{MV}}{\text{m}}$ have been measured, which does not lead to significant heating of the surface according to Fig. 4, and it is therefore possible that some other mechanism lies behind them.

4. Conclusions

The electronic effects which cause the dynamic change of temperature in the tip, exposed to a high electric field, were successfully included in an MD algorithm. The model accounts for dynamic changes of both tip geometry and temperature and gives an accurate and detailed view of the temperature development, including the temperature gradient, in tips.

Comparisons with analytic predictions show that the implemented electronic effects are needed to obtain correct temperatures and that vastly overestimated heating rates are obtained if electronic conduction is not included.

For nanosized field emitters, it is critical to account for finite size effects since both electric and thermal conductivity have a strong size dependence at this scale. Failing to account for finite size effects leads to an underestimation of the final temperature a tip will reach when a given electric field is applied.

Acknowledgements

This research was supported by the European Commission under the FP7 Research Infrastructures project EuCARD (Grant No. 227579) and the Finnish Centre of Excellence in Computational Molecular Science (CMS), financed by The Academy of Finland and the University of Helsinki.

References

- [1] H.H. Braun, S. Döbert, I. Wilson, W. Wuensch, Phys. Rev. Lett. 90 (22) (2003) 224801, doi:10.1103/PhysRevLett.90.224801.
- [2] A. Descoedres, T. Ramsvik, S. Calatroni, M. Taborelli, W. Wuensch, Phys. Rev. ST Accel. Beams 12 (3) (2009) 032001, doi:10.1103/PhysRevSTAB.12.032001.
- [3] I. Mikhailovskij, N. Wanderka, V. Storizhko, V. Ksenofontov, T. Mazilova, in: iFES 2008, Proceedings of the 51th International Field Emission Symposium, Ultramicroscopy 109 (5) (2009) 480–485, doi:10.1016/j.ultramic.2008.12.003.
- [4] R.M.I.G. Brown, J.E. Galvin, Appl. Phys. Lett. 47 (4) (1985) 358–360, doi:10.1063/1.96163.
- [5] B. Jüttner, J. Phys. D: Appl. Phys. 34 (17) (2001) R103.
- [6] E.A. Litvinov, G.A. Mesyats, D.I. Proskurovskir, Sov. Phys. Uspekhi 26 (2) (1983) 138.
- [7] A. Descoedres, Y. Levinsen, S. Calatroni, M. Taborelli, W. Wuensch, Phys. Rev. ST Accel. Beams 12 (9) (2009) 092001, doi:10.1103/PhysRevSTAB.12.092001.
- [8] C.J. Edgcombe, U. Valdre, J. Microscopy 203 (2001) 188.
- [9] G.C. Kokkorakis, A. Modinos, J.P. Xanthakis, J. Appl. Phys. 91 (7) (2002) 4580.
- [10] H. Timko, K. Matyash, R. Schneider, F. Djurabekova, K. Nordlund, A. Hansen, A. Descoedres, J. Kovermann, A. Grudiev, W. Wuensch, S. Calatroni, M. Taborelli, Contrib. Plasm. Phys. 51 (1) (2011) 5–21, doi:10.1002/ctpp.201000504.
- [11] A. Caro, M. Victoria, Phys. Rev. A 40 (5) (1989) 2287–2291, doi:10.1103/PhysRevA.40.2287.
- [12] I. Koponen, Phys. Rev. B 47 (21) (1993) 14011.
- [13] K. Nordlund, L. Wei, Y. Zhong, R.S. Averback, Phys. Rev. B (Rapid Comm.) 57 (1998) 13965–13968.
- [14] C. Björkas, K. Nordlund, Nucl. Inst. Methods Phys. Res. B 267 (2009) 1830–1836.
- [15] K. Nordlund, M. Ghaly, R. Averback, M. Caturla, T.D. de la Rubia, J. Tarus, Phys. Rev. B 57 (13) (1998) 7556–7570.
- [16] M. Ghaly, K. Nordlund, R. Averback, Philos. Mag. A 79 (4) (1999) 795–820, doi:10.1080/01418619908210332.
- [17] M.J. Sabochick, N.Q. Lam, Phys. Rev. B 43 (7) (1991) 5243.
- [18] E.L. Murphy, R.H. Good, Phys. Rev. 102 (6) (1956) 1464–1473, doi:10.1103/PhysRev.102.1464.
- [19] R.G. Forbes, Appl. Phys. Lett. 89 (11) (2006) 113–122, doi:10.1063/1.2354582.
- [20] R.G. Forbes, Surf. Interf. Anal. 36 (5–6) (2004) 395–401, doi:10.1002/sia.1900.
- [21] K. Jensen, J. Appl. Phys. 102 (2) (2007).
- [22] J.D. Jackson, Classical Electrodynamics, Wiley, 1975.
- [23] R.G. Forbes, J. Appl. Phys. 104 (8) (2008) 084303, doi:10.1063/1.2996005.
- [24] R.A. Matula, J. Phys. Chem. Ref. Data 8 (4) (1979) 1147–1298, doi:10.1063/1.555614.
- [25] C.E. Schuster, M.G. Vangel, H.A. Schafft, Microelectron. Reliab. 41 (2) (2001) 239–252, doi:10.1016/S0026-2714(00)00227-4.
- [26] A.E. Yarimbiyik, H.A. Schafft, R.A. Allen, M.E. Zaghoul, D.L. Blackburn, Implementation of simulation program for modeling the effective resistivity of nanometer scale film and line interconnects, NIST Internal Report NISTIR-7234, 2006.
- [27] A.E. Yarimbiyik, H.A. Schafft, R.A. Allen, M.D. Vaudin, M.E. Zaghoul, Microelectron. Reliab. 49 (2) (2009) 127–134, doi:10.1016/j.microrel.2008.11.003.
- [28] H.H. Mende, G. Thummes, Appl. Phys. A: Mater. Sci. Process. 6 (1) (1975) 93–97, doi:10.1007/BF00883555.
- [29] P. Heszler, L. Landström, M. Lindstam, J.O. Carlsson, J. Appl. Phys. 89 (7) (2001) 3967.
- [30] P. Heino, E. Ristolainen, Microelectron. J. 34 (9) (2003) 773–777, doi:10.1016/S0026-2692(03)00149-6.
- [31] B. Feng, Z. Li, X. Zhang, J. Appl. Phys. 105 (10) (2009) 104315, doi:10.1063/1.3129707.
- [32] B. Feng, Z. Li, X. Zhang, Thin Solid Films 517 (8) (2009) 2803–2807, doi:10.1016/j.tsf.2008.10.116.
- [33] R. Elliott, A. Gibson, Solid State Physics, Nature-Macmillan Physics, Macmillan, 1974.
- [34] A. Grudiev, S. Calatroni, W. Wuensch, Phys. Rev. ST Accel. Beams 12 (10) (2009) 102001, doi:10.1103/PhysRevSTAB.12.102001.
- [35] A.E. Yarimbiyik, H.A. Schafft, R.A. Allen, M.E. Zaghoul, D.L. Blackburn, Microelectron. Reliab. 46 (7) (2006) 1050–1057, doi:10.1016/j.microrel.2005.09.004.
- [36] R.G. Forbes, C.J. Edgcombe, U. Valdrè, Ultramicroscopy 95 (2003) 57–65, doi:10.1016/S0304-3991(02)00297-8.
- [37] F. Djurabekova, S. Parviainen, K. Nordlund, Phys. Rev. E 83 (2) (2011) 026704, doi:10.1103/PhysRevE.83.026704.
- [38] W.H. Press, S.A. Teukolsky, W.T. Vetterling, B.P. Flannery, Numerical Recipes in Fortran, second ed., vol. 1, Cambridge University Press, 1992.
- [39] R. Berman, Thermal Conduction in Solids, Oxford University Press, 1976.
- [40] L. Rayleigh, Proc. Roy. Soc. Lond. 29 (1879) 71–89.
- [41] M.E.T. Molaes, A.G. Balogh, T.W. Cornelius, R. Neumann, C. Trautmann, Appl. Phys. Lett. 85 (22) (2004) 5337–5339, doi:10.1063/1.1826237.